AUTOMATIC CO-REGISTRATION OF MULTI-TEMPORAL LANDSAT-8/OLI AND SENTINEL-2A/MSI IMAGES

S. Skakun[1,2], *J.-C. Roger*[1,2], *E. Vermote*[2], *C. Justice*[1], *J. Masek*[3]

[1] Department of Geographical Sciences, University of Maryland, College Park MD 20742, USA

[2] NASA Goddard Space Flight Center Code 619, Greenbelt, MD 20771, USA

[3] NASA Goddard Space Flight Center Code 618, Greenbelt, MD 20771, USA

Introduction

- Many applications in climate change and environmental and agricultural monitoring rely heavily on the exploitation of **multi-temporal** satellite imagery

- Combined use of freely available Landsat-8 and Sentinel-2 images can offer **high temporal frequency** of about 1 image every 3–5 days globally

- Data should be consistent
  - Including **co-registration**

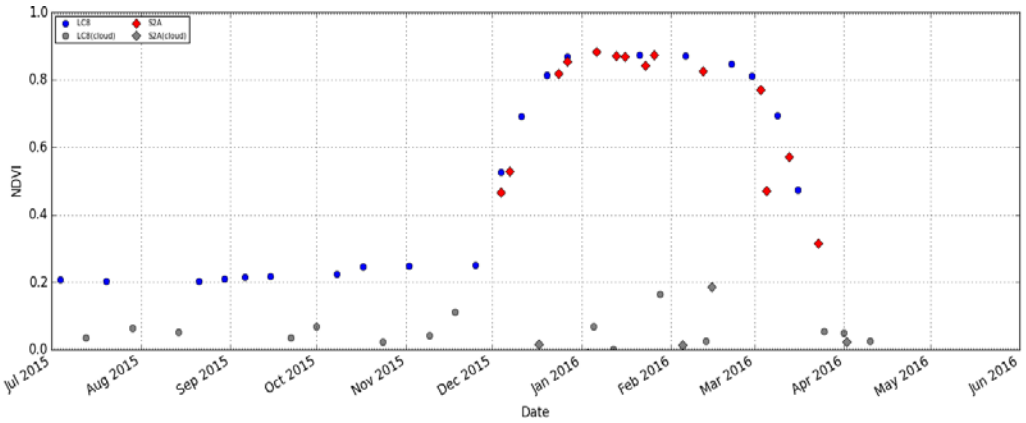

Introduction: Sentinel-2A/MSI

- MSI = Multi-Spectral Instrument

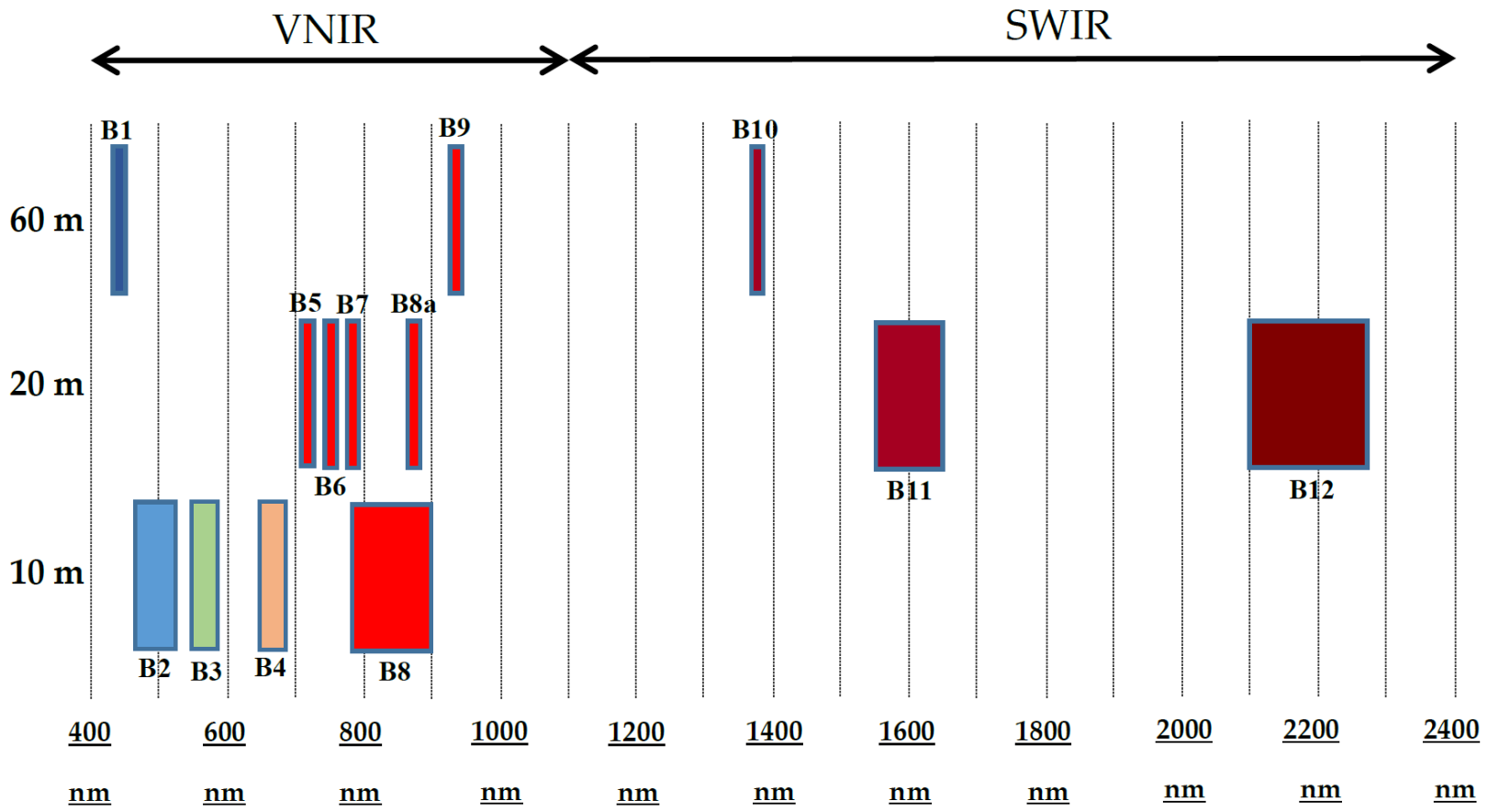

(Gascon et al. 2017)

Introduction: Landsat-8

- Operational Land Imager (OLI) and Thermal Infrared Sensor (TIRS) instruments

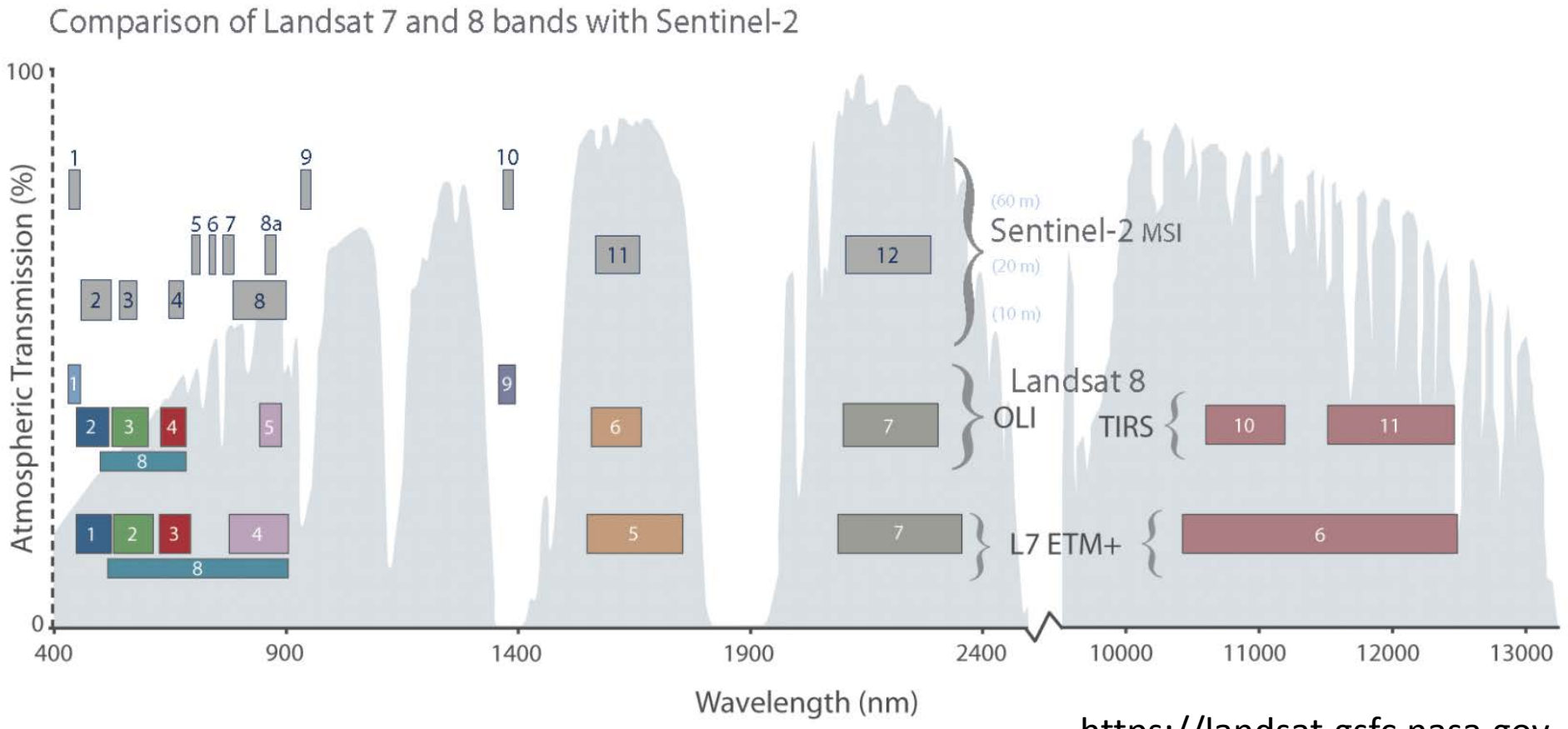

https://landsat.gsfc.nasa.gov

Introduction

- Both sensor geolocation systems are designed to use **ground control** to **improve the geolocation accuracy and repeatability** (Storey et al. 2016)

- **Sentinel-2A**
  - The Sentinel-2 geolocation will use a **Global Reference Image (GRI)** derived from orthorectified Sentinel-2 cloud-free images (Déchoz et al. 2015)
  - Planned to be available at the end of 2017

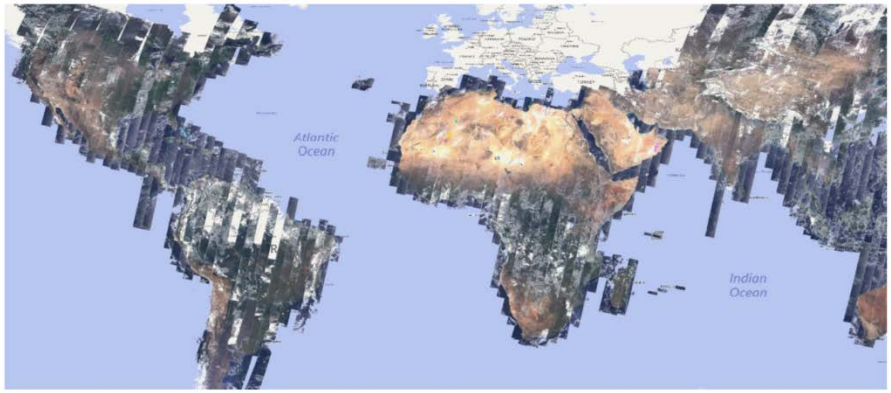

Figure 17. Overview of the Sentinel-2 GRI selection, July 2016 (European GRI products are not present on this map, since they were produced in the In-Orbit Commissioning Review (IOCR) context, in October 2015).

(Gascon et al. 2017)

- **Landsat-8**
  - The Landsat-8 geolocation uses a global sample of ground control points (Storey et al., 2014) derived for each WRS-2 path/row of circa 2000 **Global Land Survey (GLS)** Landsat-7 imagery (Gutman et al., 2013).

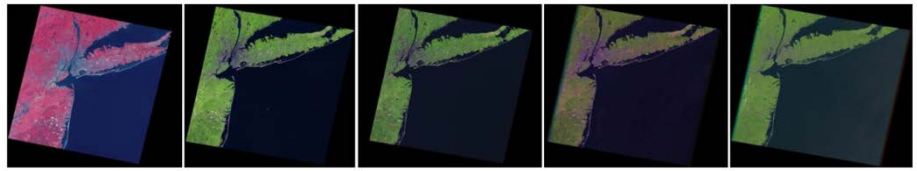

These images of New York City, New York and surrounding areas are examples of the Global Land Surveys (GLS) data sets. From left: GLS1975, GLS1990, GLS2000, GLS2005, and GLS2010.

https://landsat.usgs.gov/global-land-surveys-gls

Landsat-8/Sentinel-2A Harmonization

- Pixel value misalignment
  - LC8 (center) and S2 (UL)
- Different UTM zones:
  - L8 uses north zone even for southern hemisphere, while S2 uses south zones
    - e.g. 20N from LC8 vs 20S from S2
- Misregistration
  - **"estimate of the expected Sentinel-2 to Landsat-8 misregistration …. yields a 38 meter (2σ) expected registration accuracy between the sensors"** [*Storey et al., RSE, 2016*]

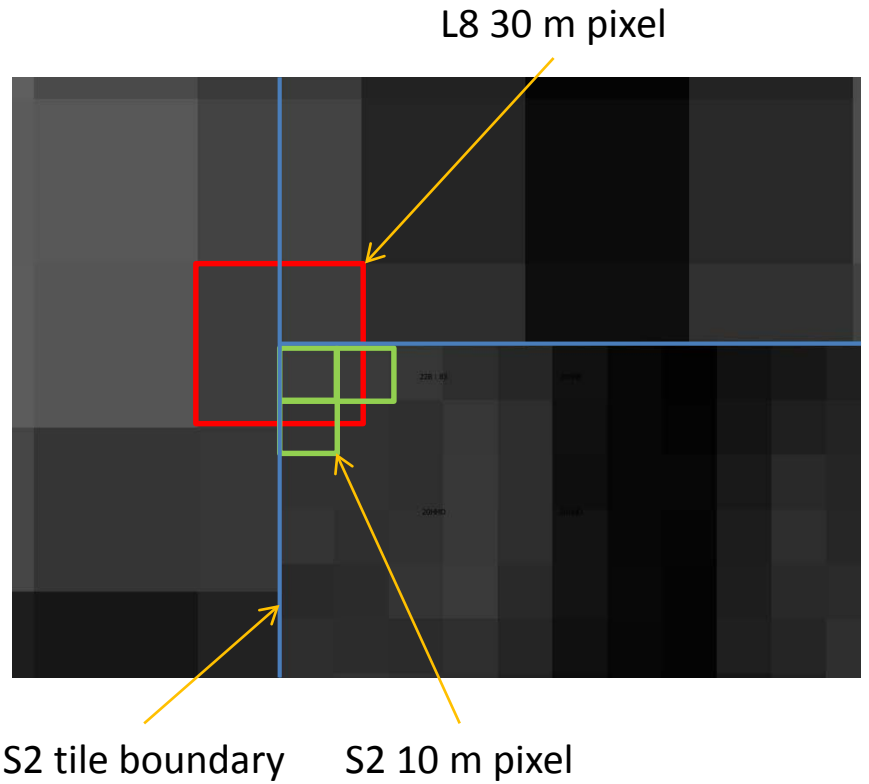

Landsat-8/Sentinel-2A Misregistration

T20HNH – Sentinel-2A, band 08 (NIR), 10 m – Landsat-8, band5 (NIR), 30 m

Methodology

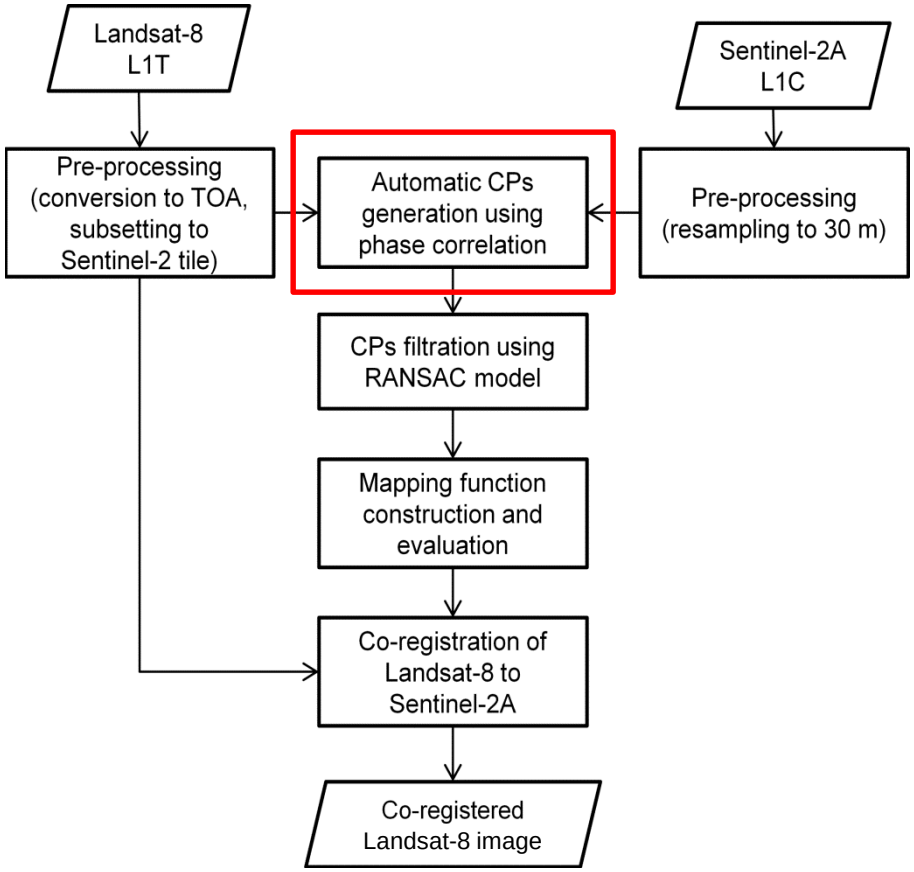

- **Automatic generation of control points (CPs).**
  - **Phase-only correlation** image matching method introduced by Guizar-Sicairos et al. (2008).
  - It uses:
    - a **cross-correlation** approach in the **frequency domain** by means of the Fourier transform and
    - exploits a computationally efficient procedure based on nonlinear optimization and Discrete Fourier Transforms (DFTs) to detect **sub-pixel shifts** between reference and sensed images.

S. Skakun, J.-C. Roger, E. F. Vermote, J. G. Masek, and C. O. Justice, "Automatic sub-pixel co-registration of Landsat-8 Operational Land Imager and Sentinel-2A Multi-Spectral Instrument images using phase correlation and machine learning based mapping," *Int. J. Digital Earth*, 2017, doi:10.1080/17538947.2017.1304586.

Methodology

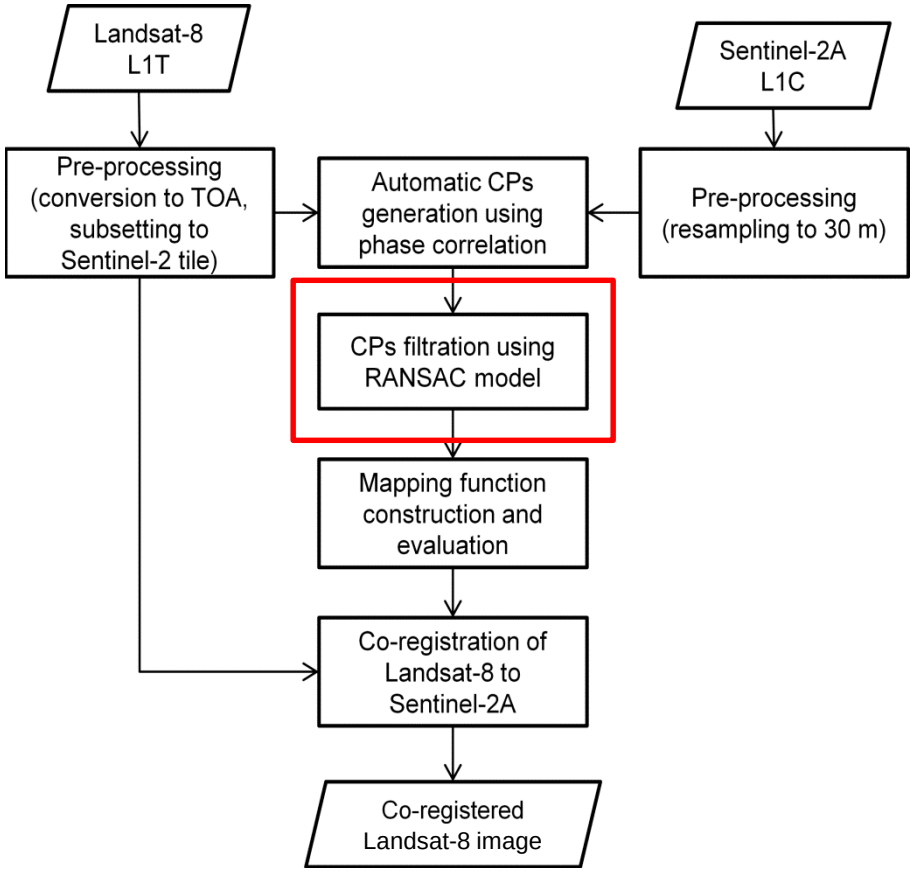

- **CPs filtering**.
  - A peak cross-correlation normalized **magnitude** is used for initial rejection of CPs.
  - After that, a RANdom SAmple Consensus (**RANSAC**) algorithm (Fischler and Bolles 1981) is run for the linear transformation model to detect inliers and outliers

S. Skakun, J.-C. Roger, E. F. Vermote, J. G. Masek, and C. O. Justice, "Automatic sub-pixel co-registration of Landsat-8 Operational Land Imager and Sentinel-2A Multi-Spectral Instrument images using phase correlation and machine learning based mapping," *Int. J. Digital Earth*, 2017, doi:10.1080/17538947.2017.1304586.

Methodology

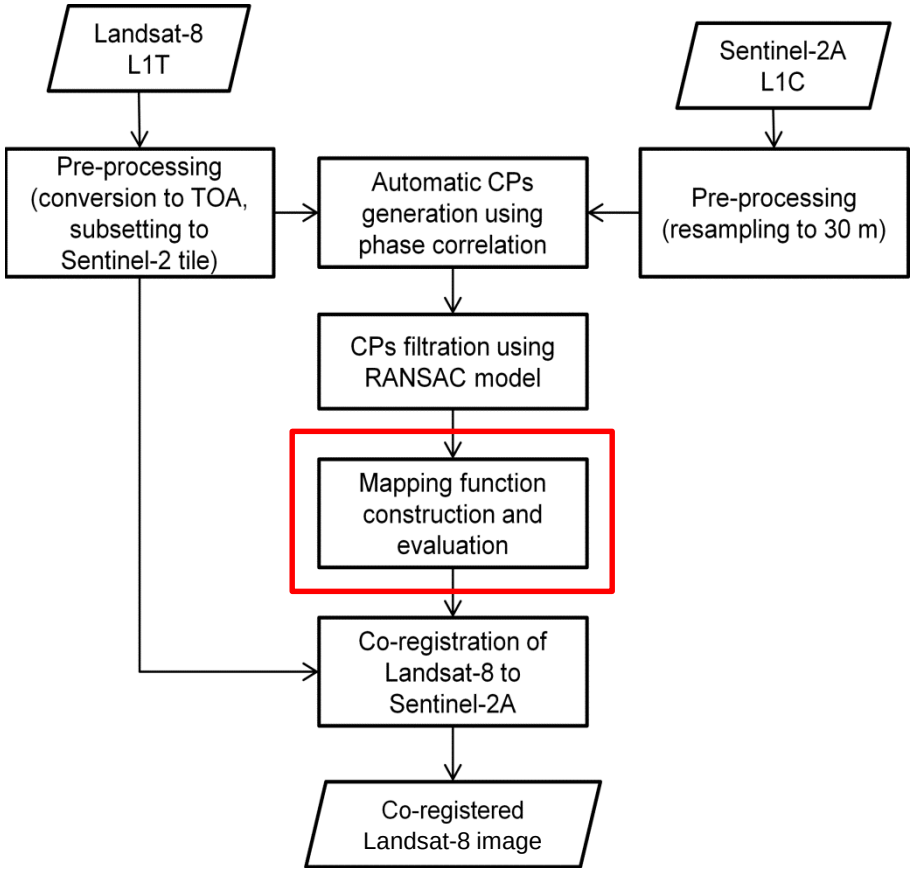

- **Transformation function**.
  - A transformation function $F()$ is built to find correspondence between CPs in the reference image $\mathbf{x}_r = (x_r, y_r)$ and points in the sensed image $\mathbf{x}_s = (x_s, y_s)$: $(x_s, y_s) = F(x_r, y_r)$.
  - The following functions are evaluated:
    - **Polynomial**
    - **Radial Basis Functions (RBFs)**
      - Gaussian
      - Thin-plate splines (TPS)
    - **Random Forest (RF)** regression

S. Skakun, J.-C. Roger, E. F. Vermote, J. G. Masek, and C. O. Justice, "Automatic sub-pixel co-registration of Landsat-8 Operational Land Imager and Sentinel-2A Multi-Spectral Instrument images using phase correlation and machine learning based mapping," *Int. J. Digital Earth*, 2017, doi:10.1080/17538947.2017.1304586.

Data used

- Co-registration of **45 Landsat-8 to Sentinel-2A pairs** and **37 Sentinel-2A to Sentinel-2A pairs** were analyzed.

Table 1. Description of data used in the study.

Country	Tile number	Acquisition date of Sentinel-2A reference image	Acquisition dates of Landsat-8 co-registered images	Acquisition dates of Sentinel-2A co-registered images
Argentina	20HNH	2015358	2015354, 2015185, 2015201, 2015242, 2015249, 2015258, 2015290, 2015306, 2015329, 2015338, 2015345, 2015361, 2016021, 2016037, 2016053	2015341, 2016006, 2016013, 2016016, 2016023, 2016026, 2016036, 2016043, 2016046, 2016063, 2016065, 2016073, 2016083, 2016093, 2016096
Argentina	20HPH	2015358	2015242, 2015258, 2015290, 2015306, 2015338, 2015354, 2016021, 2016037, 2016053	2016003, 2016013, 2016023, 2016043, 2016063, 2016073, 2016083, 2016093
US (Texas)	14SKF	2016012	2015245, 2015261, 2015293, 2015309, 2015325, 2015341, 2015357, 2016024, 2016040, 2016056, 2016072, 2016088, 2016104	2016042, 2016072, 2016132
Ukraine	36UUU	2016169	2016076, 2016092, 2016108, 2016156, 2016172, 2016188	2016096, 2016109, 2016119, 2016156, 2016166, 2016179, 2016196, 2016199, 2016206
Ukraine	34UFU	2016198	2016063, 2016182	2016048, 2016208

Note: Acquisition dates are given in the format YY YY DOY (where DOY is the day of the year).

Results

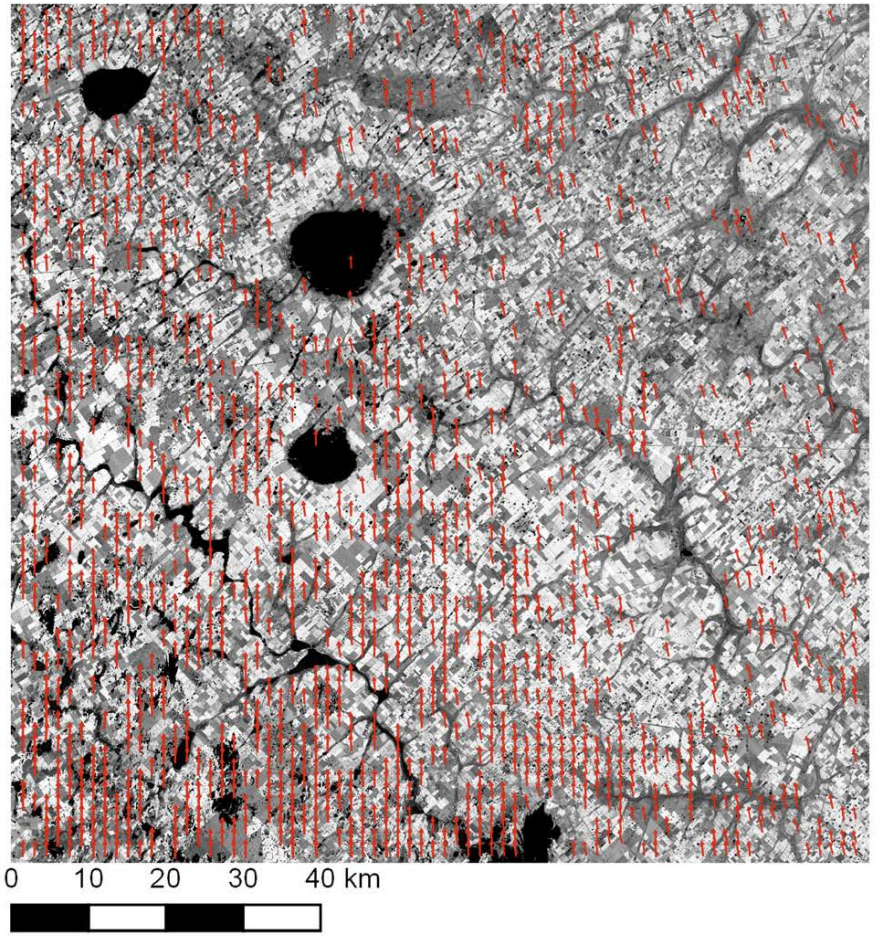

Figure 3. Location of CPs shown in the form of vectors outlining the direction and magnitude of shifts (Δ_x and Δ_y (Equation (2)) found between Landsat-8 image acquired on 2016021 (21-Jan-2016), and Sentinel-2A image acquired on 2015358 (24-Dec-2015) and used as a reference image, over the study area in Argentina, tile T20HNH. Vector lengths were multiplied by 100 for visual clarity. Overall, 1634 CPs were found using the phase-correlation approach in this case. The background is a Landsat-8 TOA NIR (band 5) image with TOA reflectance values scaled from 0.05 to 0.65.

Results

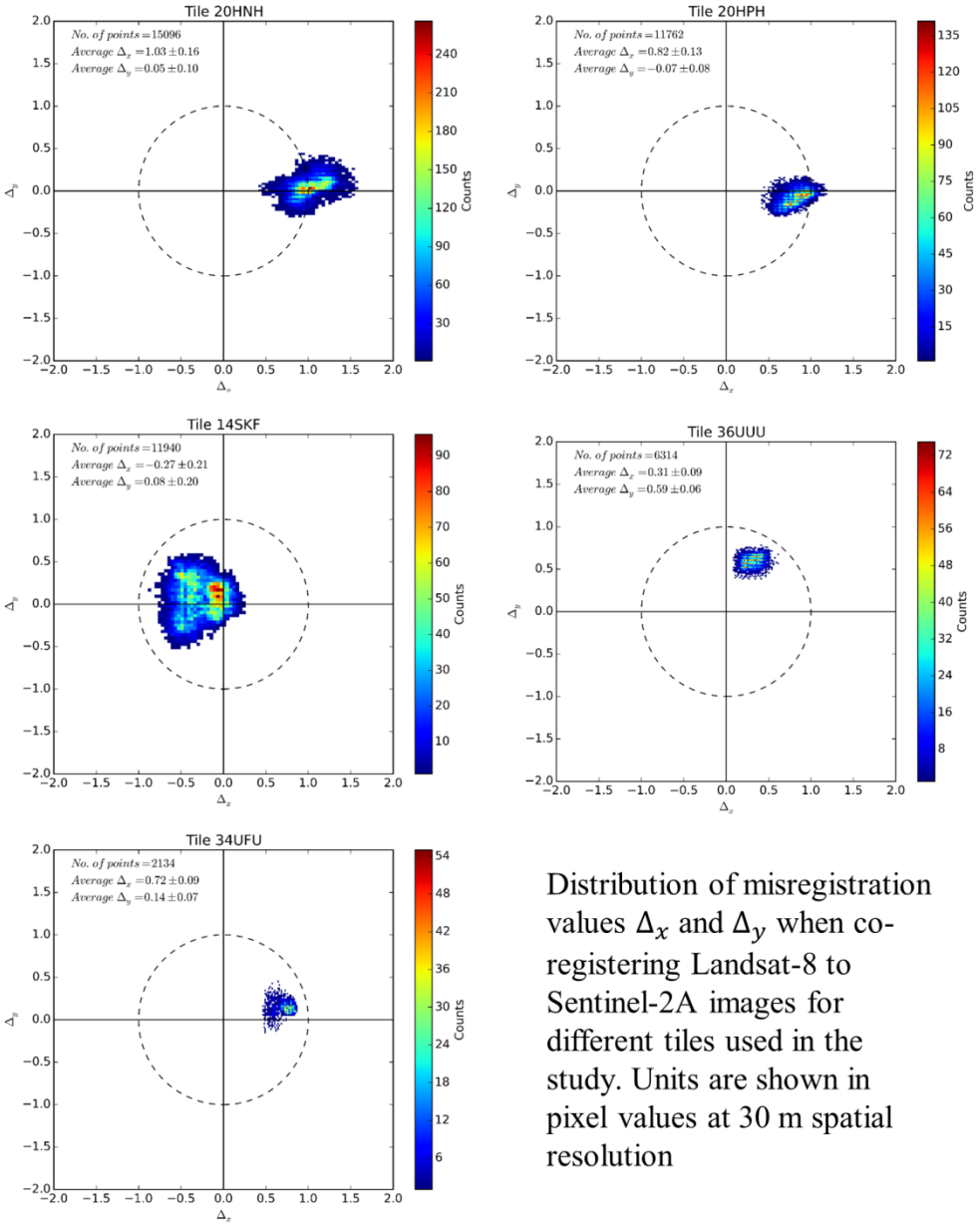

Distribution of misregistration values Δ_x and Δ_y when co-registering Landsat-8 to Sentinel-2A images for different tiles used in the study. Units are shown in pixel values at 30 m spatial resolution

Results

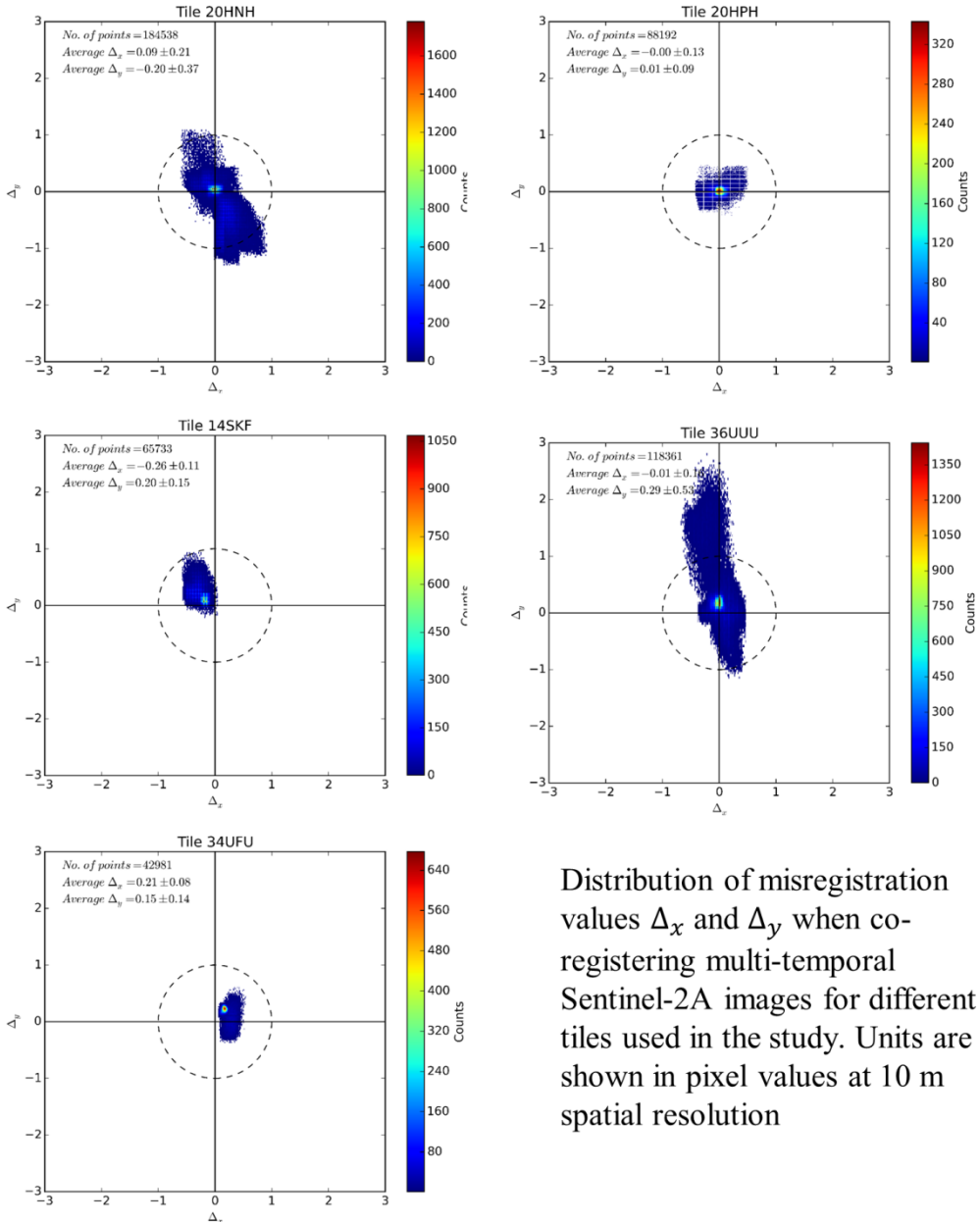

Distribution of misregistration values Δ_x and Δ_y when co-registering multi-temporal Sentinel-2A images for different tiles used in the study. Units are shown in pixel values at 10 m spatial resolution

Results

- Performance of different transformation functions when co-registering Landsat-8 to Sentinel-2A at 30 m

Table 4. Average and standard deviation of the RMSE error (Equation (4)) calculated for different transformation functions using CPs from testing set when co-registering Landsat-8 and Sentinel-2A images.

	Translation (Equations (7)–(8))		1st order polynomial (Equations (9)–(10))		Gaussian RBFs (Equations (11)–(12), (13))		RF regression		TPS (Equations (11)–(12), (14))	
Tile	Mean	Standard deviation	Mean	Standard deviation	Mean	Standard deviation	Mean	Standard deviation	Mean	Standard deviation
20HNH	0.119	0.031	0.091	0.026	0.093	0.027	0.084	0.024	0.090	0.025
20HPH	0.123	0.014	0.078	0.016	0.081	0.017	0.073	0.018	0.079	0.018
36UUU	0.108	0.011	0.072	0.015	0.074	0.015	0.059	0.014	0.073	0.015
14SKF	0.145	0.037	0.094	0.018	0.095	0.018	0.074	0.018	0.094	0.017
34UFU	0.095	0.045	0.056	0.034	0.060	0.038	0.044	0.030	0.054	0.033

Note: RMSE values are shown in pixel units at 30 m spatial resolution.

Results

- Performance of different transformation functions when co-registering Sentinel-2A to Sentinel-2A at 10 m

Table 5. Average and standard deviation of the RMSE error (Equation (4)) calculated for different transformation functions using CPs from testing set when co-registering multi-temporal Sentinel-2A images from the same orbit.

	Translation (Equations (7)–(8))		1st order polynomial (Equations (9)–(10))		Gaussian RBFs (Equations (11)–(12), (13))		RF regression		TPS (Equations (11)–(12), (14))	
Tile	Mean	Standard deviation	Mean	Standard deviation	Mean	Standard deviation	Mean	Standard deviation	Mean	Standard deviation
20HNH	0.141	0.104	0.125	0.076	0.125	0.076	0.105	0.060	0.126	0.074
20HPH	0.133	0.064	0.128	0.062	0.127	0.062	0.114	0.059	0.129	0.064
36UUU	0.181	0.126	0.114	0.046	0.114	0.046	0.088	0.035	0.112	0.048
14SKF	0.133	0.066	0.123	0.050	0.118	0.046	0.089	0.036	0.123	0.051
34UFU	0.122	0.101	0.092	0.086	0.091	0.084	0.066	0.059	0.093	0.088

Note: RMSE values are shown in pixel units at 10 m spatial resolution.

Table 6. The same as Table 5, but for adjacent Sentinel-2A orbits.

	Translation (Equations (7)–(8))		1st order polynomial (Equations (9)–(10))		Gaussian RBFs (Equations (11)–(12), (13))		RF regression		TPS (Equations (11)–(12), (14))	
Tile	Mean	Standard deviation	Mean	Standard deviation	Mean	Standard deviation	Mean	Standard deviation	Mean	Standard deviation
20HNH	0.239	0.048	0.207	0.031	0.202	0.028	0.164	0.032	0.205	0.031
36UUU	0.248	0.212	0.191	0.139	0.189	0.138	0.138	0.087	0.193	0.142

Results

Without co-registration

With co-registration

T20HNH – Sentinel-2A, band 08 (NIR), 10 m – Landsat-8, band5 (NIR), 30 m

Results

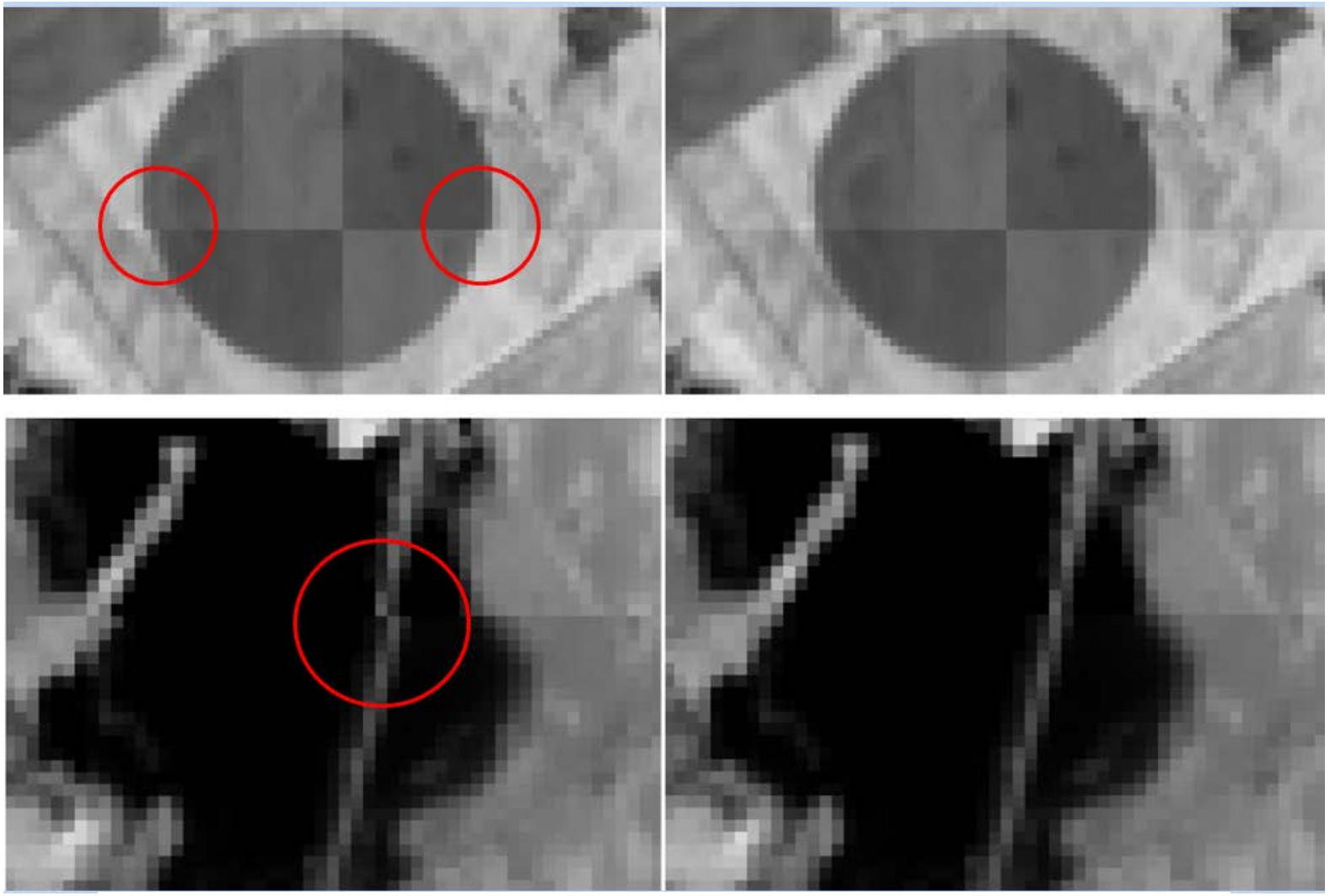

A 30 m “chessboard” composed of alternating Landsat-8 (acquired on 20-Dec-2015) and Sentinel-2A (24-Dec-2015) images before (left) and after co-registration (right).

Sentinel-2A Multi-spectral Misregistration

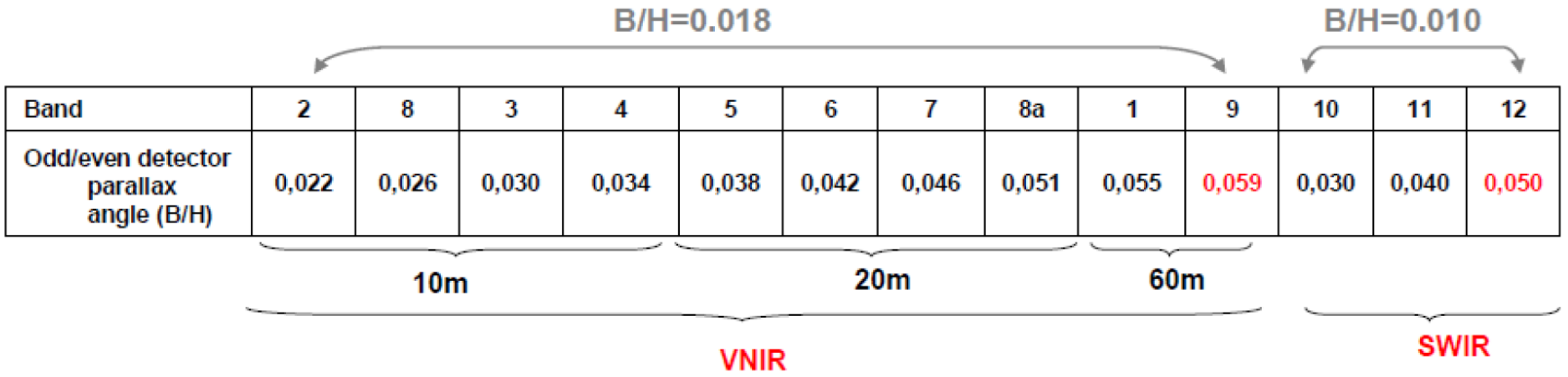

Figure 2: Staggered detector configuration and inter-detector/inter-band parallax angles

[Sentinel-2 Products Specification Document https://sentinel.esa.int/documents/247904/685211/Sentinel-2-Product-Specifications-Document]

Sentinel-2A Multi-spectral Misregistration

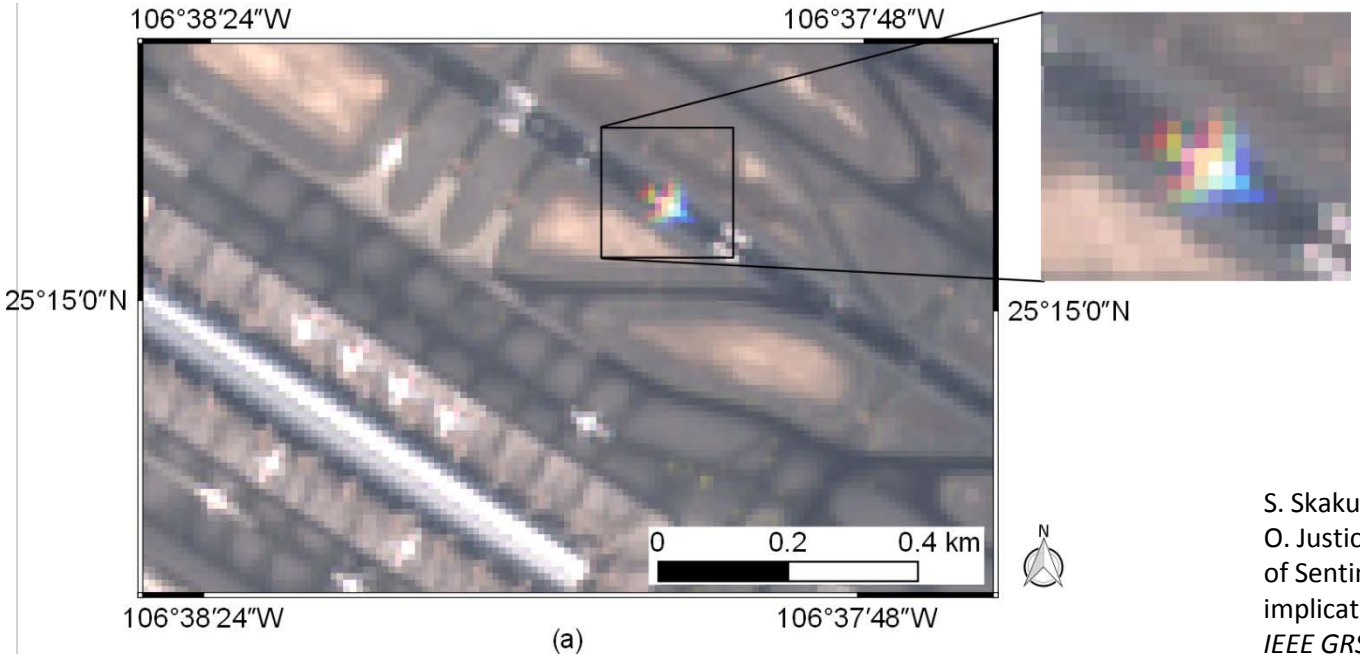

S. Skakun, E. F. Vermote, J.-C. Roger, and C. O. Justice, "Multi -spectral misregistration of Sentinel -2A images: analysis and implications for potential applications ," *IEEE GRSL*, 2017, (under review)

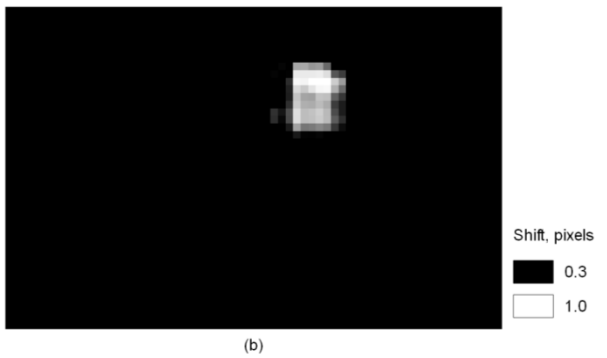

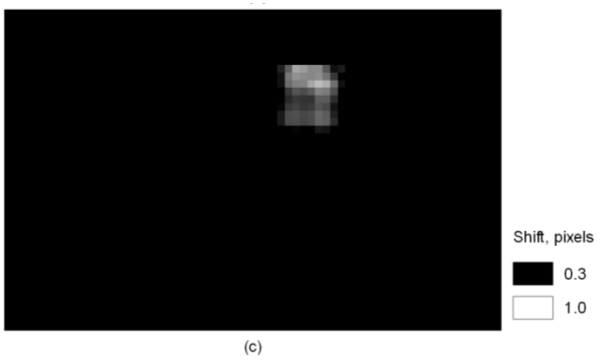

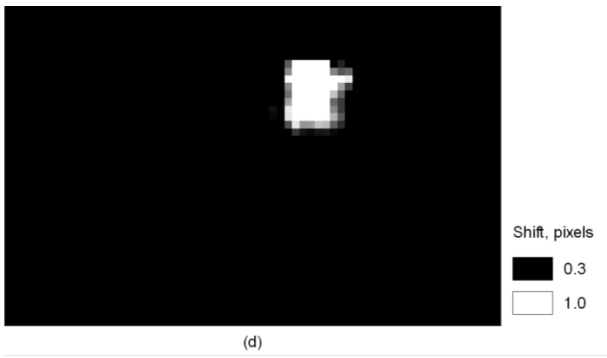

A subset of Sentinel-2A true color image (combination of bands B4, B3, and B2) acquired on 13 June 2017 (a). Shift maps were estimated from different pairs of visible bands at 10 m spatial resolution using a phase correlation approach with a sliding window size *nw*=16 and step size *ns*=2: bands 3 and 2 (b); bands 4 and 3 (c); and bands 4 and 2 (d).

Sentinel-2A Multi-spectral Misregistration

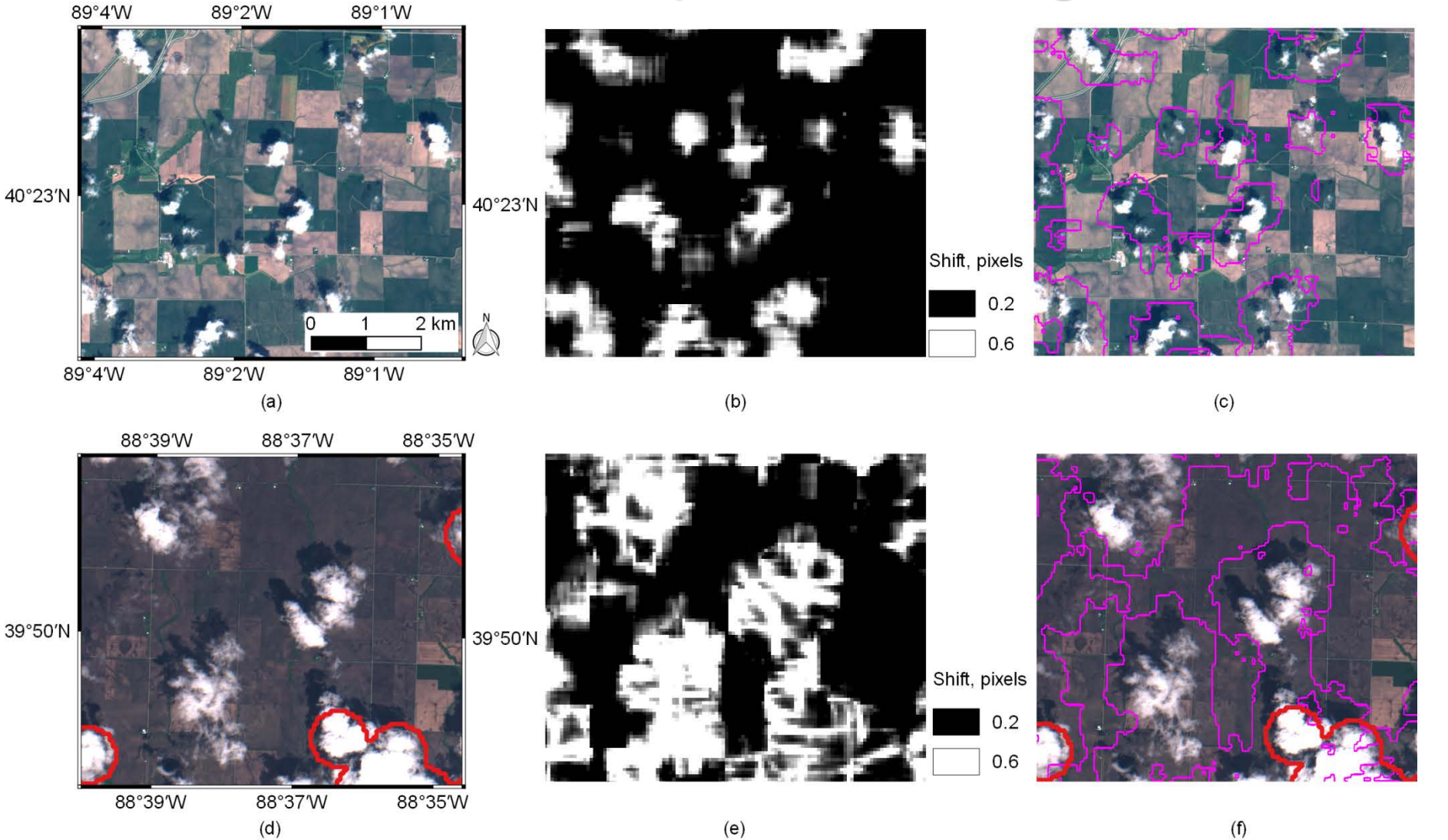

Example of cloud detection for Sentinel-2A/MSI images acquired over the US (tile 16TCK) on 15 June 2016 (a) and 21 May 2017 (d). True color images (combination of bands 4, 3 and 2) at 10 m spatial resolution along with the built-in cloud mask (in red) are shown in subplots (a) and (d); shifts estimated from band 4 and 2 images using phase correlation are shown in (b) and (e); cloud masks (in magenta) derived from the multi-spectral misregistration using a threshold of 0.2 pixels for shifts are shown in subplots (c) and (f).

Conclusions

- **Phase correlation** proved to be a robust approach that allowed us to identify 100's and 1000's of control points on Landsat-8/Sentinel-2A images acquired more than 100 days apart.

- **Misregistration** of up to **1.6 pixels** at **30 m** resolution between multi-temporal **Landsat-8** and **Sentinel-2A** images, and **1.2 pixels** (**same orbits**) and **2.8 pixels** (**adjacent orbits**) at **10 m** resolution between multi-temporal **Sentinel-2A** images were observed.

- The **Random Forest** regression used for constructing the **mapping function** showed best results, yielding an average RMSE error of **0.07 ± 0.02 pixels** at **30 m**, and **0.09 ± 0.05** at **10 m**

- Sentinel-2A multi-spectral misregistration:
  - shifts of more than **1.1 pixels** can be observed for **moving targets** such as airplanes
  - sub-pixels shifts of **0.2 to 0.8 pixels** are observed for **clouds**, and can be used for cloud detection as one of the criteria

Thank You!